Showcasing research from Professor XiuJun (James) Li's laboratory, Department of Chemistry & Biochemistry, University of Texas at El Paso, Texas, USA.

Smart paper transformer: new insight for enhanced catalytic efficiency and reusability of noble metal nanocatalysts

Although noble metal nanocatalysts show superior performance to conventional catalysts, they can be problematic when balancing catalytic efficiency and reusability. To address this dilemma, we for the first time developed a smart paper transformer (s-PAT) to support nanocatalysts, based on the facile phase conversion between paper and pulp. The pulp phase was used to maintain high catalytic efficiency and the transformation to paper enabled their high reusability. Additionally, a novel chromatography paper-supported Au nanosponge catalyst as an example of paper transformers was developed to demonstrate high-efficiency and high-reusability environmental catalysis.

As featured in:

See XiuJun Li *et al.*,
Chem. Sci., 2020, **11**, 2915.

ROYAL SOCIETY
OF **CHEMISTRY**

rsc.li/chemical-science

ROYAL SOCIETY OF CHEMISTRY

Smart paper transformer: new insight for enhanced catalytic efficiency and reusability of noble metal nanocatalysts†

Qijie Jin, [ab] Lei Ma,[a] Wan Zhou, [a] Yuesong Shen,[b] Olivia Fernandez-Delgado[a] and XiuJun Li [*acd]

Although noble metal nanocatalysts show superior performance to conventional catalysts, they can be problematic when balancing catalytic efficiency and reusability. In order to address this dilemma, we developed a smart paper transformer (s-PAT) to support nanocatalysts, based on easy phase conversion between paper and pulp, for the first time. The pulp phase was used to maintain the high catalytic efficiency of the nanocatalysts and the transformation to paper enabled their high reusability. Herein, as an example of smart paper transformers, a novel chromatography paper-supported Au nanosponge (AuNS/pulp) catalyst was developed through a simple water-based preparation process for the successful reduction of *p*-nitrophenol to demonstrate the high catalytic efficiency and reusability of the noble metal nanocatalyst/pulp system. The composition, structure, and morphology of the AuNS/pulp catalyst were characterized by XRD, TGA, FE-SEM, ICP, TEM, FT-IR, and XPS. The AuNS/pulp catalyst was transformed into the pulp phase during the catalytic reaction and into the paper phase to recover the catalysts after use. Owing to this smart switching of physical morphology, the AuNS/pulp catalyst was dispersed more evenly in the solution. Therefore, it exhibited excellent catalytic performance for *p*-nitrophenol reduction. Under optimal conditions, the conversion rate of *p*-nitrophenol reached nearly 100% within 6 min and the k value of AuNS/pulp (0.0106 s^{-1}) was more than twice that of a traditional chromatography paper-based catalyst (0.0048 s^{-1}). Additionally, it exhibited outstanding reusability and could maintain its high catalytic efficiency even after fifteen recycling runs. Accordingly, the unique phase switching of this smart paper transformer enables Au nanosponge to transform into a highly efficient and cost-effective multifunctional catalyst. The paper transformer can support various nanocatalysts for a wide range of applications, thus providing a new insight into maintaining both high catalytic efficiency and reusability of nanocatalysts in the fields of environmental catalysis and nanomaterials.

Introduction

Nanomaterials have attracted increased attention in multiple disciplines due to their unique size and shape effects.[1–4] As an important member of nanomaterials, noble metal nano-catalysts (Au nanoclusters, Pd nanoparticles, Pt nanoparticles, *etc.*) have widespread applications in many fields, such as environmental catalysis,[5–7] photothermal therapy,[8–10] carbon–carbon coupling reactions,[11–13] *etc.* Among these applications, their use in environmental catalysis is of significant importance due to its ecological value, specifically in water treatment. So far, Fe$_3$O$_4$@SiO$_2$–Ag,[14] Au@SiO$_2$,[15] Au/TiO$_2$,[16] AgNPs/SiNSs,[17] Pd/C$_3$N$_4$,[18] and many other noble metal nanocatalysts have been used for water treatment. However, the selection of noble metal catalysts often faces a dilemma: it is difficult to achieve both high catalytic efficiency and high reusability at the same time. Catalysts for water treatment can be divided into two categories: liquid-phase catalysts and solid-phase catalysts. Liquid-phase catalysts exhibit high catalytic efficiency, but it is challenging to separate them from wastewater after use. For instance, Au/TiO$_2$, Au colloidal solutions and water-soluble Pd-8 nano-clusters exhibited high catalytic performance for *p*-nitrophenol (4-NP) reduction but were difficult to recover, resulting in low reusability.[19–21] On the other hand, solid-phase catalysts have high reusability but the catalytic efficiency is substantially lower than that of liquid phase catalysts.[22] Although Pd/MoS$_2$ can be

[a]*Department of Chemistry and Biochemistry, University of Texas at El Paso, El Paso, Texas 79968, USA. E-mail: xli4@utep.edu*

[b]*College of Materials Science and Engineering, Nanjing Tech University, Nanjing 210009, PR China*

[c]*Biomedical Engineering, Border Biomedical Research Center, University of Texas at El Paso, El Paso, Texas 79968, USA*

[d]*Environmental Science and Engineering, University of Texas at El Paso, El Paso, Texas 79968, USA*

† Electronic supplementary information (ESI) available. See DOI: 10.1039/c9sc05287a

reused 5 times, it needs 10 min to complete the 4-NP reduction reaction (k value = 0.386 min^{-1}, lower than that of many liquid phase catalysts).[23] Additionally, noble metal nanomaterials easily aggregate, which further causes a decrease in catalytic efficiency.[24,25] Therefore, the concurrent increase in catalytic efficiency and reusability is imperative for the application of noble metal nanocatalysts but is difficult. Fe_3O_4 supported noble metal nanocatalysts ($Au–Fe_3O_4@MOF$,[26] $Pt–Fe_3O_4@$-graphene[27]), which controlled the recycling process with their magnetic properties, were reported in some literature to exhibit both high catalytic efficiency and reusability. Lignin supported Ag (Ag@LPAH) also exhibited high catalytic efficiency and stability.[28] However, their complex preparation processes and the high cost limit their applications. Although the synergistic effects between Ag, Au, and CuO resulted in excellent catalytic performance for the catalytic reduction of p-nitrophenol, the reusability was still limited (3 cycles) and Au–Ag/CuO still needed to consume a lot of precious metals and metal oxides.[29]

As an active ingredient, the Au nanomaterial is an excellent electron donor or acceptor, so it has the capacity to promote catalytic reactions by the redox cycle process significantly. It also exhibits excellent chemical inertness and can remain stable under various reaction conditions.[30] Therefore, Au nanomaterials are excellent catalysts in catalytic reactions.[31] Among different Au nanostructures, the Au nanosponge (AuNS) has a three-dimensional open architecture exposing a large number of catalytically active sites.[32] The large surface-to-volume ratio and the presence of numerous active sites are beneficial resulting in superior catalytic activity.[33] In addition, unlike AuNPs,[34] AuNS does not require the addition of protective capping agents to avoid aggregation. The properties and characteristics of AuNS result in the formation of a robust and high-efficiency catalyst.

Along with catalysts, catalyst carriers, such as graphene oxide,[35] TiO_2,[36] polymers[37] and cellulose, also play a vital role in efficient catalytic reactions.[38] Chromatography paper consisting of cellulose microstructures (micro-sized diameter) can be used as a 3D catalyst carrier with highly effective surface areas.[39,40] Furthermore, the paper has the unique property where its liquid (*i.e.* pulp) and solid phases can be easily and reversibly switched. When paper is transformed into pulp, the pulp can be uniformly suspended in water increasing the contact area between catalysts and reactants, and hence improving the catalytic efficiency. On the other hand, when the pulp is dried, it will become the solid phase (*i.e.* the so-called paper). The catalyst is captured on the solid paper and thus can be easily recovered. The paper-supported catalysts can be used many times by repeating this process, allowing for excellent reusability. Thus, the smart paper transformer (s-PAT) provides an extraordinary solution to address a vital problem of current noble metal catalysts by unifying both high efficiency and high reusability. That is to say, chromatography paper or filter paper is an excellent catalytic carrier for noble metal nanocatalysts. Furthermore, paper has abundant –OH functional groups on the cellulose surface which ensure strong binding strength between paper and Au nanomaterials and that the nanocatalyst cannot be washed away. Although chromatography paper has

been used as a catalyst carrier before,[41,42] the unique phase-transformation properties of paper (switching easily between paper and pulp) have not been utilized.

Given the aforementioned features of s-PAT, the smart paper transformer can enable chromatography paper supported noble metal nanocatalysts such as AuNS (AuNS/pulp) to exhibit high catalytic efficiency and high reusability. To verify the hypothesis, the catalytic reduction of p-nitrophenol (4-NP), a water pollutant, was chosen as a model for the application of the AuNS/pulp catalyst in water treatment. It is well known that 4-NP is a significant contributor to worsening environmental problems such as water contamination resulting in mutagens, teratogens, carcinogens, *etc.*[43] Alternatively, p-aminophenol (4-AP), the catalytic reaction product, is an important intermediate with widespread applications in various fields including anti-pyretic drugs, photographic developers, corrosion inhibitors, and hair-dying agents.[44–46] With the increase of environmental protection awareness and increasingly strict environmental protection laws,[29] developing new efficient and economical technologies to degrade 4-NP has great ecological and environmental significance and important economic value.[47,48] Herein, s-PAT was used to support AuNS for the catalytic reduction of nitroaromatic compounds. A series of characterization tests confirmed that the AuNS/pulp catalyst exhibits not only higher catalytic efficiency than various solid-phase catalysts, but also higher reusability than liquid phase catalysts. The conversion rate of 4-NP reached nearly 100% within 6 min under optimal conditions while the catalytic efficiency remained high even after 15 recycling runs. The microstructure of the chromatography paper was retained during the processes of AuNS preparation and catalytic reactions. This discovery provides a new platform to seek efficient and economical catalysts for various applications in environmental remediation, biomass conversion, nanomaterials, and so on.

Experimental

Materials

Sodium borohydride ($NaBH_4$, 98%) was purchased from Alfa Aesar (Tewksbury, MA). p-Nitrophenol (4-NP) was purchased from EMD Millipore Corporation (Billerica, MA). Gold (III) chloride trihydrate ($HAuCl_4 \cdot 3H_2O$) was acquired from Sigma (St. Louis, MO). Chromatography paper (Whatman #1) with 240 mm diameter and 180 μm thickness was purchased from Whatman (Maidstone, England). Water with a resistivity of 18.2 MΩ cm @ 25 °C from a Millipore Milli-Q system (Bedford, MA) was used to prepare the solutions. All chemicals were of analytical grade and used without further processing.

Catalyst preparation

A simple water-based preparation process was used to prepare the AuNS/pulp catalyst. Schemes 1 and S1† present the preparation process and application of the AuNS/pulp nanocatalyst. Firstly, the chromatography paper was cut into squares with dimensions of 1 × 1 cm^2 by using a Laser cutter (Zing 16-30 W, Epilog, America). Then, 160 mg $HAuCl_4 \cdot 3H_2O$ was added into

Scheme 1 Schematic of the preparation (left) and application (right) processes of the s-PAT supported AuNS/pulp catalyst.

4 mL ultrapure water to obtain a $HAuCl_4$ yellow clarified solution. Secondly, 16 pieces of chromatography paper (138 mg) and the $HAuCl_4$ solution were mixed together in a 20 mL vial and maintained under vigorous stirring for 4 h in the dark. The pulp was formed after stirring. Thirdly, 90 mg of $NaBH_4$ was dissolved into 3 mL ultrapure water. Then the $NaBH_4$ solution was added into the pulp rapidly under continuous vigorous stirring for 1 h to completely reduce Au^{3+} to Au^0. Finally, the resulting black pulp suspension was washed and centrifuged three times with water to obtain purple pulp with AuNS in it. After this the pulp was dried at 60 °C for 6 h and the s-PAT supported Au catalyst was obtained and stored at room temperature before use.

Catalytic activity measurement

The catalytic efficiency of the s-PAT supported AuNS/pulp catalyst was investigated by applying it in 4-NP conversion to *p*-aminophenol (4-AP). Firstly, an appropriate amount of the AuNS/pulp catalyst was dissolved in 3 mL ultrapure water and stirred for 30 min so that the AuNS/pulp catalyst could take the form of pulp. Secondly, the 4-NP solution (1 mM, 5 mL) and a fresh $NaBH_4$ solution (0.1 M, 5 mL) that was stored in a refrigerator were added to the vial and mixed together. Then, the mixed solution was added into the pulp suspension rapidly while vigorously stirring. Afterward, 100 μL mixed solutions were pipetted into a 96 well microplate (Thermo Fisher Scientific, America). The absorbance spectra of the solutions in the microplate were obtained using a multi-mode microplate reader (Microplate Reader M3, Molecular Devices, San Jose, CA). The value of total organic carbon (TOC) was recorded using a total organic carbon analyzer. The remaining fraction of 4-NP (X) was calculated using eqn (1).

$$X = C_t/C_0 \times 100\% \tag{1}$$

where C_0 is the initial 4-NP concentration and C_t is the concentration at different time intervals (t). Furthermore, the AuNS/pulp catalyst was recycled 16 times to investigate the reusability. For each recycling, the used catalyst was washed, centrifuged and dried for the next experiment.

Characterization

X-ray diffraction (XRD) patterns were obtained on an X-ray diffractometer (Empyrean Series 2, PANalytical, Netherlands). The scan speed was $5° \cdot min^{-1}$ and the 2θ scans covered 10–85°. The microstructural nature was investigated using a field emission scanning electron microscope (FE-SEM, S-4800, Hitachi, Japan) and transmission electron microscopy (TEM, JEOL, JEM-2010UHR). The element distribution was investigated by electron mapping. Fourier transform infrared (FT-IR) spectra were obtained using a Nicolet Nexus 670 series FT-IR spectrophotometer in ATR mode. The spectra were recorded under ambient conditions over the range of 750–4000 cm^{-1} with a resolution of 0.5 cm^{-1}. Thermogravimetric analysis was performed using a TGA system (Mettler Toledo International Inc, America). Before the test, the sample was dried at 80 °C for 2 h and a ceramic crucible was pre-treated by a high-temperature sintering process. The 0.5 mg sample was placed in the ceramic crucible and kept in the auto-sampler of the TGA system. Then the sample was heated from 30 °C to 800 °C at a 5 °C min^{-1} heating rate. The gas flow rate of the nitrogen atmosphere was 20 mL min^{-1}. The X-ray photoelectron spectroscopy (XPS) patterns were acquired using a PHI 5600 spectrometer with a hemispherical energy analyzer (Mg-Kα radiation, 1253.6 eV), and the vacuum degree was maintained at 10^{-7} Pa. The samples were dried at 80 °C for 24 h to remove moisture and then were tested without surface treatment. Curve fitting was performed by utilizing XPSPEAK 4.1 with a Shirley-type background.

Results and discussion

Catalytic reduction of 4-NP

In the experiment of the catalytic reduction of 4-NP, the yellow color of the 4-NP/$NaBH_4$ solution faded and ultimately became bleached with the addition of the s-PAT supported AuNS/pulp catalyst. The fading time related to the catalytic reduction of 4-NP to 4-AP decreased with the increase of the catalyst amount. As a result, the effect of the catalyst amount was investigated by UV-Vis spectrophotometry (Fig. 1). As shown in Fig. 1(a)–(d), the intensity of the representative peak of 4-NP in the presence of $NaBH_4$ at 400 nm decreased and that of the representative peak of 4-AP at 295 nm increased gradually with time. Early literature also confirmed that the peaks at 400 nm and 295 nm represented 4-NP and 4-AP, respectively.[49] The linear relationship between the absorbance and 4-NP concentration was calculated based on Fig. S1.† It was also noted that the value of TOC showed no noticeable changes at different times (Fig. S2†), indicating the transformation from 4-NP to 4-AP instead of the benzene ring when the AuNS/pulp catalyst was added into the 4-NP/$NaBH_4$ solution. However, there were no obvious spectral changes at 400 nm in the absence of the AuNS/pulp catalyst or in the presence of only the chromatography paper (*i.e.* no AuNS) in the reaction solution (Fig. 1(b) and (c) insets), though the slight decrease in Fig. 1(c) was observed at the beginning of the reaction due to the physical adsorption on the porous paper material. A visual inspection of this experiment also shows that
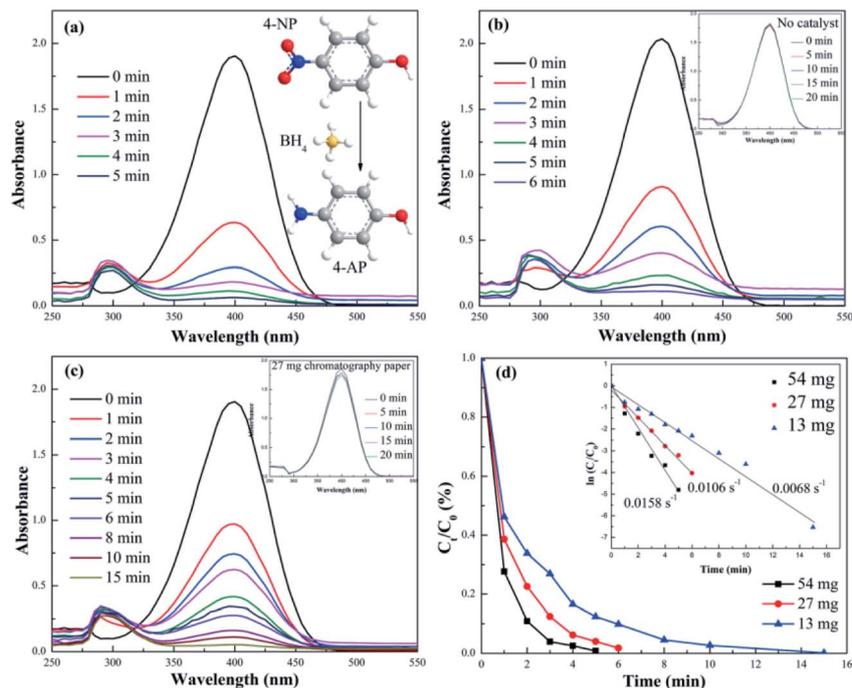
Fig. 1 UV–vis absorption spectra of 4-NP reduction in the presence of (a) 54 mg AuNS/pulp catalyst, (b) 27 mg AuNS/pulp catalyst, and (c) 13 mg AuNS/pulp catalyst. (d) C_t/C_0 vs. time plot. The insets in (b) and (c) show the spectra of the solution in the absence of the AuNS/pulp catalyst and AuNS (i.e. only in the presence of paper but not AuNS).

the color of the 4-NP/NaBH$_4$ solution showed no changes for a few days in the absence of the catalyst, indicating that the transformation from 4-NP to 4-AP could not occur in the presence of NaBH$_4$ alone, as confirmed in the literature.[50] It was reported that the transformation from 4-NP to 4-AP was favourable thermodynamically but unfavourable kinetically without the catalyst.[40] In other words, the pristine chromatography paper had no catalytic activity and the AuNS was the principal active component in the AuNS/pulp catalyst for 4-NP degradation.

The AuNS amount plays an important role in the catalytic reduction reaction. The catalytic efficiency decreased gradually when the AuNS/pulp amount decreased from 54 to 13 mg. Fig. 1(d) shows the 4-NP conversion over time with varying amounts of the catalyst. The conversion rate reached 89.1% within 2 min and nearly 100% within 5 min when the amount of the AuNS/pulp catalyst was 54 mg. This conversion rate was higher than that in many previous reports.[51,52] When the amount of the AuNS/pulp catalyst decreased to 27 mg, the catalyst still exhibited satisfactory catalytic reactions and the conversion rate could still reach 98.3% within 6 min. The high catalytic efficiency of the AuNS/pulp catalyst was largely attributed to the porous structure of the AuNS and the uniform distribution of the AuNS catalyst in solutions by the pulp phase of the s-PAT. It is known that the porous structure could promote the adsorption and activation of reactive molecules on the active sites of the catalyst, thereby improving the catalytic performance. However, solid-phase catalysts often fail to achieve high efficiency due to the lack of uniform distribution of

catalysts. A more detailed comparison of the catalytic efficiency between the pulp phase and the paper phase will be discussed in the following section of this article.

The catalytic reduction reaction from 4-NP to 4-AP follows first-order kinetics because of the excessive amount of NaBH$_4$. The kinetics was calculated using eqn (2).

$$\ln(C_t/C_0) = -kt \qquad (2)$$

where C_0 is the initial 4-NP concentration, C_t is the concentration at different time intervals (t) and k is the apparent rate constant of the reaction. Fig. 1(d) shows the first-order kinetic curves of 4-NP over AuNS/pulp with different catalyst amounts. The data points followed basic linearity, which was slightly different from that in previous literature.[41] This was a result of vigorous stirring during the catalytic reactions eliminating bubbles produced in the vial. Thus, it prevented bubbles from blocking the interaction between the catalyst and reactants. Furthermore, the catalytic performance improved with the increase of the AuNS amount so that the value of k was 0.0158, 0.0106 and 0.0068 s^{-1} for 54, 27 and 13 mg catalysts, respectively. However, considering the efficiency and the cost, 27 mg was chosen as the optimum catalyst amount.

To investigate the effect of the NaBH$_4$ concentration on catalytic activity, UV–vis absorption spectra for different NaBH$_4$ concentrations were collected and the results are shown in Fig. S3† and 2. As shown in Fig. S3,† the reaction time increased gradually with the decrease of the NaBH$_4$ concentration. When the concentration of NaBH$_4$ was 0.01 M, the catalytic efficiency was very low taking about 25 min for the reaction to be
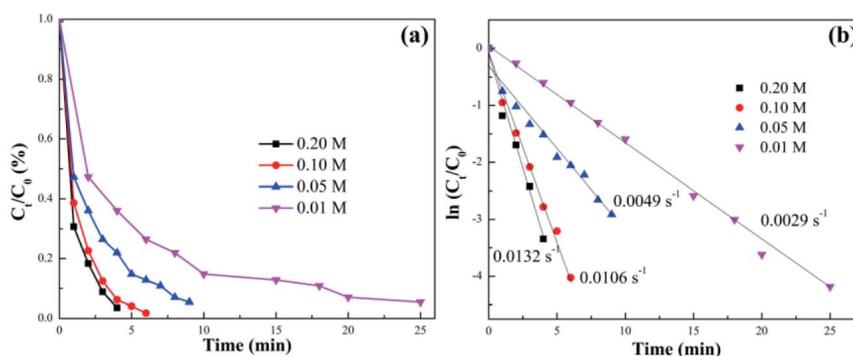
Fig. 2 (a) The C_t/C_0 and (b) $\ln(C_t/C_0)$ vs. time plots in the presence of different concentrations of NaBH$_4$ over the AuNS/pulp catalyst.

completed. When the NaBH$_4$ concentration was increased from 0.01 M to 0.05 M (NaBH$_4$/4-NP molar ratios of 10 to 50, respectively), the reaction time decreased to 9 min. However, increasing the NaBH$_4$/4-NP molar ratio to higher than 100 did not have a significant effect on the catalytic efficiency. For instance, when the NaBH$_4$ concentrations were 0.20 and 0.10 M (the molar ratios were 200 and 100), the corresponding reaction times were 4 and 6 min, respectively. Fig. 2 displayed the first-order kinetic curves of 4-NP over AuNS/pulp with different NaBH$_4$ concentrations. It can be observed that the NaBH$_4$ concentration could affect the catalytic efficiency significantly, especially when the molar ratio was less than 100. The value of k increased from only 0.0029 s^{-1} to 0.0049 s^{-1} when the concentration of NaBH$_4$ was increased from 0.01 to 0.05 M. On the other hand, no great changes were observed with the increase of the 4-NP concentration (Fig. S4†). The difference in reaction time was only within 1–2 min when the 4-NP concentration was increased exponentially. In other words, the NaBH$_4$ concentration and not the 4-NP concentration was the main influencing factor when the other conditions were the same. Therefore, it can be speculated that the first step of the transformation from 4-NP to 4-AP (Au transfers NaBH$_4$ to active hydrogen species) was the key process to control the reaction time during the catalytic reduction.

Catalytic efficiency and reusability of the paper transformer-supported nanocatalysts

Although solid-phase catalysts can be readily recycled due to their high reusability, they have a lower catalytic efficiency than liquid-phase catalysts due to the amount of time it takes for the reactants to reach the catalyst surface. The s-PAT's transformation from the paper phase to the pulp phase enables uniform distribution of catalysts in a solution, providing solid-phase catalysts with a smart strategy for high-efficiency catalysis. Table S1† lists the correlated data of 4-NP reduction under different conditions. Both the catalytic efficiency and the economic cost would increase correspondingly with higher catalyst amounts and higher NaBH$_4$ concentrations. The increase of the 4-NP concentration could reduce the economic cost but it would increase the reaction time. Considering both catalytic efficiency and economic factors, 27 mg of the catalyst, 0.10 M NaBH$_4$, and 1 mM 4-NP were determined to be optimum conditions. Under the optimal conditions, the conversion rate could reach 95% within 4.5 min and nearly 100% within 6 min. To compare the reported data for the catalytic reduction of p-nitrophenol, different catalysts are shown in Table 1.[53–55] The k value of AuNS/pulp was calculated using 13 mg catalyst and the value was found to be 0.0068 s^{-1}. It can be observed that the catalytic efficiency was higher if the catalysts (such as Au/SnNb$_2$O$_6$) could be evenly dispersed in water while the reusability was better for the solid-phase catalysts (e.g. graphene/PDA-Au, Ni@PtNi NSc-rGO, and Ag/CH-FP). Among these catalysts, only our AuNS/pulp catalyst exhibited both high catalytic efficiency (k value 0.0068 s^{-1}) and outstanding reusability (15 recycling runs). In other words, the smart switching between pulp and paper guaranteed the combination of high catalytic efficiency and outstanding reusability of the AuNS/pulp catalyst platform. As shown in Fig. 1(d), by increasing the catalyst amount or the NaBH$_4$ concentration, higher catalytic efficiency

Table 1 Comparison of the catalytic conditions and efficiency of the AuNS/pulp with reported data[a]

Catalyst	TOF (min^{-1})	k (s^{-1})	4-NP (μmol)	NaBH$_4$/4-NP ratio	Temperature (°C)	Metal amount (μmol)	Recycling runs	Ref.
AuNS/pulp	0.158	6.8×10^{-3}	5	100	RT	21.1	15	This work
Au/SnNb$_2$O$_6$	0.106	19.4×10^{-3}	4.3	767	RT	10.1	—	53
Graphene/PDA-Au	0.384	3.7×10^{-3}	1	1320	RT	0.2	—	54
Ni@PtNi NSc-rGO	—	4.5×10^{-3}	0.5	1000	24.8	—	5	55
Ag/CH-FP	0.008	3.9×10^{-3}	2	100	RT	21.3	5	41

[a] TOF: turnover frequency.

and k values could be achieved. Furthermore, our AuNS/pulp catalyst reduced a greater amount of 4-NP, while allowing the catalyst to retain high catalytic efficiency even after many recycling runs. This is a significant advantage of our s-PAT supported AuNS/pulp catalyst.

As mentioned earlier, the s-PAT can be easily switched between the pulp and the solid paper phases. Paper being a porous material has been used to support various nanomaterials, increasing the reaction kinetics, and has also been used as a carrier for other related applications.[56,57] For instance, paper supported Ag took advantage of the porous characteristics and exhibited impressive catalytic performance.[41] To confirm the superior performance of the s-PAT to that of solid paper, we also compared different catalytic performances in 4-NP catalytic reduction between the s-PAT supported AuNS/pulp and the solid paper supported AuNS/paper.

Fig. 3 displays the different UV-vis absorption spectra for 4-NP reduction by the AuNS/pulp and AuNS/paper catalysts. It can be seen that 4-NP reduction was completed within 6 min by using AuNS/pulp, whereas it needed 18 min to be completed in the presence of AuNS/paper, which implies that the catalytic efficiency of the s-PAT supported AuNS/pulp was 300% higher than that of the solid-phase Au/paper catalyst. The AuNS/pulp could be evenly suspended in the whole reaction solution so that it significantly improved the chances of coming into contact with 4-NP in the solution, while the 4-NP reaction in Fig. 3(b) was limited by the regionally localized AuNS catalyst on paper which sank to the bottom of the solution. It can be concluded that even though both reactions contained the same amount of Au, the s-PAT supported AuNS/pulp made full use of the AuNS catalyst. In contrast, AuNS/paper, due to the restriction of nanocatalysts in a limited space in the solution, could not achieve full catalytic efficiency. According to the $\ln(C_t/C_0)$ vs.
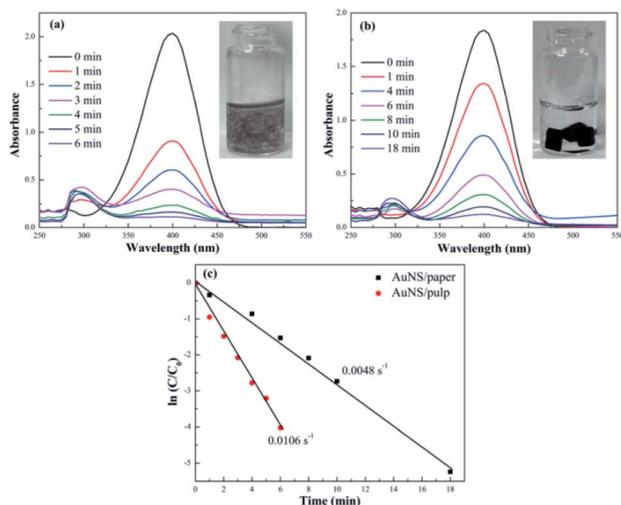
time plot in Fig. 3(c), the k value (0.0106 s^{-1}) for AuNS/pulp was 2.2 fold higher than that for AuNS/paper (0.0048 s^{-1}), further indicating the improved catalytic performance of the s-PAT supported AuNS/pulp compared to the solid paper supported AuNS/paper.

Both catalytic efficiency and reusability are important for industrial applications. As discussed earlier, liquid-phase catalysts usually provide high catalytic efficiency (such as Au/Fe$_3$O$_4$@TiO$_2$ and[58] Ag@carbon[59]), but it is extremely challenging to separate them from wastewater and recycle them for reuse. The AuNS/pulp catalyst provides a solution for this problem. When dried and transformed into the paper phase, the catalyst can be easily separated from wastewater for reuse, ensuring high reusability. Therefore, after investigating the high efficiency of the s-PAT supported catalyst, we further explored the reusability of the s-PAT supported AuNS catalyst. As shown in Fig. S5† and 4(a), the fresh AuNS/pulp catalyst achieved 98.3% conversion within 6 min and its apparent rate (k value) was 0.0106 s^{-1}. After four recycling runs, the catalyst could still exhibit almost the same efficiency as the fresh one. The k value of the AuNS/pulp catalyst in the fifth cycle (0.0102 s^{-1}) remained almost the same as that of the fresh catalyst. The catalytic efficiencies at 7 min reached 96.3% and 91.6% in the tenth and fifteenth cycles, respectively. On the other hand, most other solid catalysts can be reused for just five or ten cycles and the catalytic efficiency usually decreases below 90% or 85%.[26,50] Hence, the s-PAT supported AuNS/pulp catalyst exhibits excellent reusability and has enormous potential for various industrial applications.

Although the AuNS/pulp catalyst exhibited excellent reusability, a slight decrease in catalytic efficiency was observed with increased recycling runs. As shown in Fig. 4(a), the k value decreased from 0.0077 to 0.0056 s^{-1} from the 10th to the 15th cycles. The decrease of the catalytic efficiency was likely due to the detachment of AuNS from the catalyst support, which was confirmed in Fig. S6.† We also used ICP to verify the Au content (0.47 mg L^{-1}) in the supernatant after the catalytic reaction (Table S2†). The catalyst loss would cause the catalyst eventually to become a waste catalyst after many recycling runs. In our research, it was determined that a fresh catalyst became a waste catalyst after 16 recycling runs. Furthermore, we investigated the regeneration feasibility of a waste catalyst. For the regeneration of a waste catalyst, 45 mg waste catalyst and 4 mg HAuCl$_4$·3H$_2$O (4.4 wt% AuNPs) were added into 3 mL water to obtain the pulp solution under vigorous stirring. Then a NaBH$_4$ solution (3 mg NaBH$_4$ in 3 mL water) was quickly added to the pulp suspension to completely reduce Au^{3+} with vigorous stirring for 1 h. Finally, the as-prepared black suspended paper fibers were centrifuged and washed three times with water to obtain the purple pulp. After the purple pulp was dried at 60 °C for 6 h, the waste AuNS/pulp catalyst was regenerated.

Fig. 4(b) and S7† show the catalytic comparison for 4-NP reduction using the fresh, 16-time recycled, and regenerated AuNS/pulp catalysts. The waste catalyst (i.e. 16 cycle runs) completed the catalytic reaction within 12 min and the 4-NP conversion reached 85.3% at 6 min. Its apparent rate (k value) was only 0.0055 s^{-1}. However, the regenerated catalyst achieved 98.4% within 6 min, and its k value was recovered to 0.0104 s^{-1}.

Fig. 3 UV-vis absorption spectra for 4-NP reduction using the (a) AuNS/pulp and (b) AuNS/paper catalysts. (c) $\ln(C_t/C_0)$ vs. time plot. The insets in (a) and (b) show photographs of the catalytic reaction systems in the presence of different catalysts. AuNS/pulp enabled high uniformity of catalyst distribution in solutions compared to AuNS/paper.
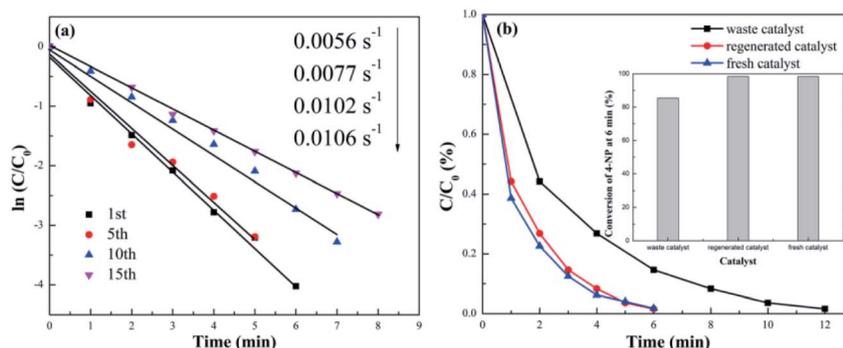
Fig. 4 (a) $\ln(C_t/C_0)$ vs. time plot for different recycling runs over the AuNS/pulp catalyst and (b) C_t/C_0 vs. time plot of the fresh, waste and regenerated catalysts.

The result for the regenerated AuNS/pulp catalyst was comparable with that for the fresh catalyst. Thus, the high catalytic efficiency can be recovered by loading a small quantity (4.4 wt%) of AuNS on a waste catalyst. In other words, the outstanding regeneration capacity of the AuNS/pulp catalyst further enhances its reusability. In summary, the s-PAT supported AuNS/pulp catalyst exhibits not only high catalytic efficiency but also outstanding reusability and regeneration capacity.

SEM and TEM analysis

We also performed FE-SEM, TEM, XRD, TGA, FT-IR, and XPS to characterize the composition, structure, and morphology of the s-PAT supported AuNS/pulp catalyst. Fig. 5 and S8† show the FE-SEM and TEM micrographs of the chromatography paper and the fresh AuNS/pulp catalyst. As shown in Fig. 5(a) and (b), the chromatography paper consisted of many long fibers with a smooth surface. From the measurement, the diameter of the fiber was found to be about 10–20 μm. As observed in Fig. 5(c) and (d), the Au nanosponge had a porous structure like a sponge and the size of the AuNS was about 50–100 nm. AuNS nanostructures clumped together and were entwined around long paper fibers. In addition, some smaller Au nanoparticles were embedded in the paper fibers, and their sizes were between 5 and 14 nm (Fig. S8†). The nano-size and porous structure of AuNS facilitated catalyst adsorption and activation of reactive molecules, thereby increasing catalyst activity. From a comparison between Fig. 5(a) and (c), it can be observed that the fiber surface of AuNS/pulp was not as smooth as that of chromatography paper, but the major microstructure looked similar between pulp and paper fibers. Some white spots

emerged from the chromatography paper but did not appear on the AuNS/pulp surface. The main reason was that the conductivity of the chromatography paper increased after the growth of AuNS. In addition, SEM was employed for element mapping on the chromatography paper and the AuNS/pulp. Fig. S9 and S10† show the element mapping results of the chromatography paper and the fresh AuNS/pulp catalyst. It can be observed that the C and O elements were well distributed on the chromatography paper surface. After AuNS preparation on paper, Au was distributed on the AuNS/pulp surface, confirming the existence and the distribution of AuNS in the pulp.

XRD and FT-IR analysis

The XRD patterns of the chromatography paper, the fresh AuNS/pulp catalyst, and the used AuNS/pulp catalyst (reused 10 times) were analyzed and the results are shown in Fig. 6(a). The crystallinity and crystallite size were calculated using the Debye–Scherrer equation (MDI Jade 5.0 software). All the reflections of the samples provided the diffraction patterns for cellulose (PDF-ICDD 50-2241) and Au (PDF-ICDD 04-0784). As shown in Fig. 6(a), the three strong peaks at $2\theta = 14.99°$, $16.49°$, and $22.78°$ were attributed to cellulose (-110), (110) and (200) diffractions, respectively. The peaks at $38.18°$, $44.39°$, $64.58°$, and $77.54°$ corresponded to the gold (111), (200), (220) and (311) diffractions. This, therefore, suggested that the chromatography paper consisted of crystalline cellulose. The crystallinity and crystallite size of cellulose crystals were 88% and 7 nm, respectively. In addition, the crystallinity and crystallite size of cellulose crystals exhibited no significant change when AuNS was prepared on the chromatography paper. In other words, the
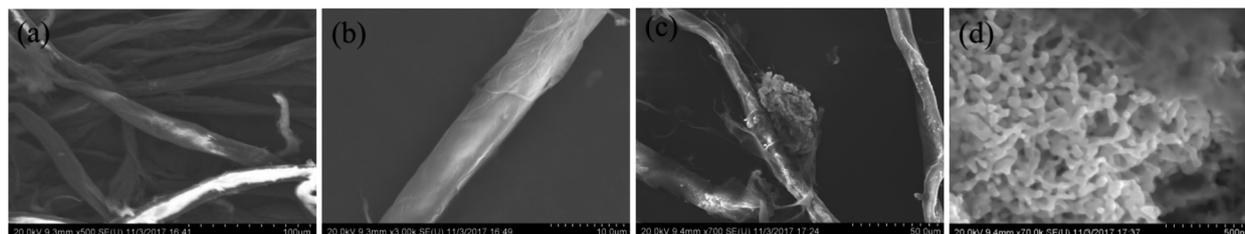

Fig. 5 SEM micrographs of (a) and (b): chromatography paper; (c) and (d): fresh AuNS/pulp.
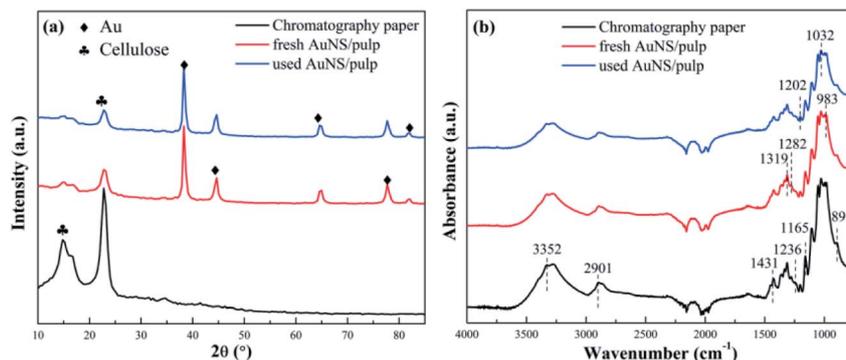
Fig. 6 (a) X-ray diffraction patterns and (b) FT-IR spectra of the chromatography paper and AuNS/pulp catalysts.

structure of the chromatography paper did not change after AuNS preparation. The intensity of the cellulose peak decreased slightly for the used AuNS/pulp catalyst compared to the fresh AuNS/pulp catalyst, suggesting a small amount of cellulose loss after use. Finally, obvious Bragg reflections of Au were observed on the fresh AuNS/pulp surface and the crystallinity and the crystallite size of Au were 95% and 18 nm, respectively. The crystallinity and crystallite size of AuNS also showed no obvious change after use, suggesting high reusability of the AuNS/pulp catalyst.

Fig. 6(b) shows the FT-IR spectra of the chromatography paper, the fresh AuNS/pulp, and the used AuNS/pulp catalyst (750–4000 cm⁻¹). It can be seen that the FT-IR spectra from the chromatography paper and the fresh and used catalysts were similar to each other and all the peaks were attributed to cellulose I. From the literature, the 3352 cm⁻¹ and 2901 cm⁻¹ peaks were attributed to O–H and C–H stretching vibrations, respectively.[60,61] The bands at 1431 cm⁻¹, 1319 cm⁻¹, and 1282 cm⁻¹ were assigned to symmetric CH₂ bending, CH₂ wagging, and C–H bending.[62,63] The bands at both 1236 cm⁻¹ and 1202 cm⁻¹ were assigned to C–O–H bending in plane at C-6.[63,64] The bands at both 1165 cm⁻¹ and 897 cm⁻¹ were assigned to C–O–C stretching at the β-glucosidic linkage.[65] The bands at both 1032 cm⁻¹ and 983 cm⁻¹ were assigned to C–O stretching vibrations at C-6.[66] Fig. 6(b) also demonstrates that the peak intensity decreased slightly with the addition of AuNS or after use. This is due to the decrease in the relative amount of cellulose, which was consistent with the XRD results. However, no peak shift was observed, suggesting that the AuNS preparation process did not alter the original interactions among cellulose chains. In other words, the porous microstructure of the chromatography paper showed no change after the AuNS preparation process, which was favourable for maintaining high catalytic efficiency after many recycling runs (see Fig. 4(a)), as discussed in an earlier section of this article.

TGA analysis

Fig. 7 displays the TGA thermograms of the chromatography paper, the fresh AuNS/pulp, and the used AuNS/pulp catalyst. No weight loss was observed until the temperature increased to 250 °C due to the sample being dried before each measurement

to eliminate moisture. An obvious weight loss was observed in the temperature range from 250 to 600 °C. This was attributed to the decomposition of, oxidation of, and evolution of gases from the main organic components (cellulose).[41,42] In addition, the degradation temperature of the AuNS/pulp catalyst decreased to 263 °C, while that of chromatography paper was 295 °C. The shift of the degradation temperature may be due to AuNS acting as a catalyst and decreasing the activation energy during the thermal event.[67–69] In addition, the weight loss of the chromatography paper increased to 90.9% while that of the fresh AuNS/pulp and used AuNS/pulp catalysts increased to 61.8% and 58.3%, respectively. This difference is due to the presence of AuNS in the fresh AuNS/pulp and used AuNS/pulp catalysts. Therefore, the amount of AuNS in the AuNS/pulp catalyst could be deduced from the difference of the weight loss. It was noted that the fresh AuNS/pulp and the used AuNS/pulp contained 32 wt% and 36 wt% AuNS, respectively. This is because there was a small amount of cellulose loss, leading to an increase in the relative amount of AuNS after many cycles of reuse.

XPS analysis

The surface composition and oxidation states of catalysts play an important role in the catalytic reduction reaction, so XPS was
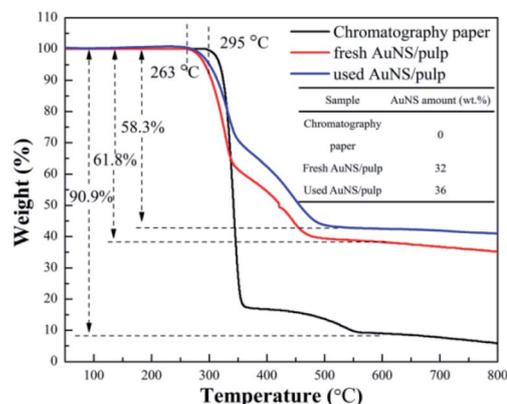

Fig. 7 TGA thermograms of the chromatography paper and the AuNS/pulp catalyst.

applied to investigate the surface properties of the s-PAT supported AuNS/pulp catalyst. XPS analysis also further verified the formation of the AuNS/pulp catalyst and the efficient removal of oxygenated functional groups of the catalyst. Fig. 8 shows the survey, O 1s, C 1s and Au 4f XPS high-resolution scan spectra of the chromatography paper and the AuNS/pulp catalysts. The O 1s peaks were deconvoluted into three peaks, two of which corresponded to cellulose: the peak centered at about 533.1 eV was attributed to the oxygen in ether groups (hereafter denoted as O_c) and the other peak centered at about 532.8 eV was attributed to the oxygen atoms in alcohol groups (hereafter denoted as O_β).[70] Furthermore, a relatively well-developed peak located between 530.4 eV and 532.8 eV could be attributed to the presence of either loosely bound oxygen or hydroxide (OH^-, hereafter denoted as O_α).[71] The intensities of the O 1s peaks decreased because the relative content of oxygen decreased after the AuNS preparation process. In addition, the O 1s peaks of AuNS/pulp showed a shift toward higher binding energy after the AuNS preparation process, indicating that there was a strong interaction between Au and O atoms. The strong interaction also guaranteed that the AuNS catalyst would not be washed away from the chromatography paper after use.

As shown in Fig. 8(c), the C 1s spectrum was divided into four peaks: (1) the peak located at 284.7 eV was attributed to the carbon bond to carbon ($C-C$, C_1); (2) the peak located at 285.3 eV was attributed to the sp^3 carbon bond to hydrogen atoms ($C-O$, C_2); (3) the peak located at 286.2 eV was attributed to the cellulose carbon bond to a single oxygen ($C=O$, C_3); (4) the peak located at 288.0 eV was attributed to the cellulose carbons bond to two oxygen atoms ($O-C=O$, C_4).[49] Similarly, AuNS

preparation on paper caused a decrease in the intensity of the C 1s peaks and the shift toward a higher binding energy. In other words, there was strong interaction among Au, C and O atoms. Fig. 8(d) shows the Au 4f XPS spectrum of the AuNS/pulp catalyst. The strong doublet peaks of Au 4f emerging at 87.6 eV and 83.9 eV were attributed to Au^0 $4f_{5/2}$ and Au^0 $4f_{7/2}$, respectively. There was also no other peak ascribed to Au^{3+}, illustrating that the reduction of Au^{3+} to Au^0 was complete after the AuNS preparation process. These observations revealed that Au^0 was the predominant species in the AuNS/pulp catalyst.

Table 2 lists the atomic ratios on the surface of the chromatography paper and the fresh AuNS/pulp catalyst. For the O element, the noticeable change was the decrease of hydroxide (O_α). The relative content of both O_β and O_c increased slightly but the increase of O_c was not so obvious. That is, the AuNS preparation process resulted in a decrease of hydroxide on the chromatography paper surface. For the C element, the relative content of C_3 increased obviously and that of C_1, C_2 and C_4 decreased after the AuNS preparation process, leading to different electron states in those different environments. We speculate that the atomic ratio changes were due to the reaction between the $C-C$ bond and hydroxide adsorbed on the chromatography paper surface during the AuNS preparation process. In addition, the hydroxyl group of the $C-O$ bond will also be consumed during the AuNS preparation process. Therefore, the cleavage of the $C-C$ and $-OH$ bond and the formation of the $C=O$ bond occurred during the AuNS preparation stage, resulting in atomic ratio changes. However, according to the other data, the overall structure of the chromatography paper was maintained during the AuNS preparation process.
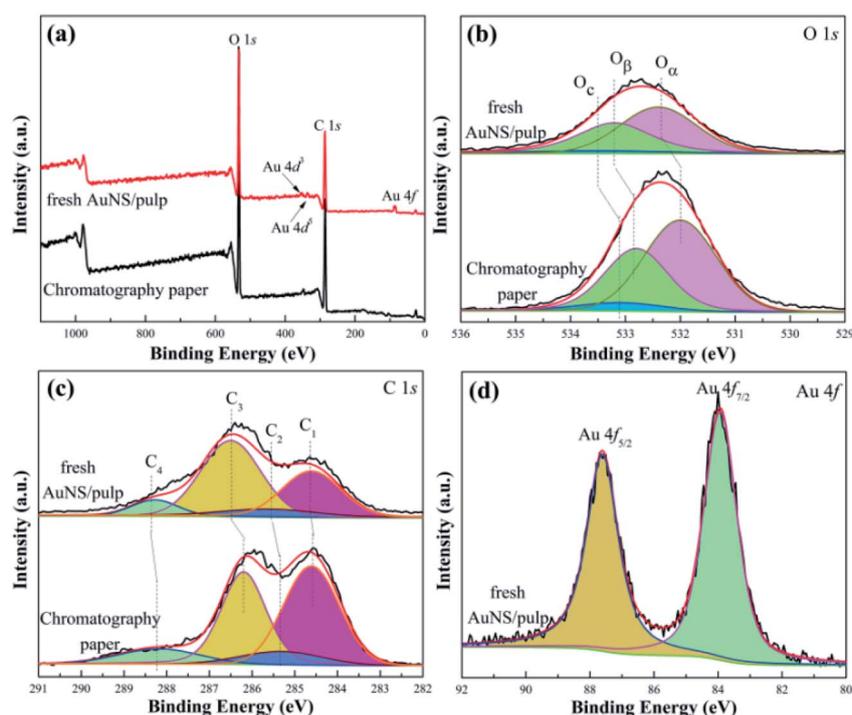

Fig. 8 (a) Survey, (b) O 1s, (c) C 1s and (d) Au 4f XPS high-resolution scan spectra of different catalyst samples.

Table 2 Atomic ratios on the surface of the chromatography paper and AuNS/pulp catalyst[a]

Sample	$O_\alpha/(O^*)$	$O_\beta/(O^*)$	$O_c/(O^*)$	$C_1/(C^*)$	$C_2/(C^*)$	$C_3/(C^*)$	$C_4/(C^*)$
Chromatography paper	0.57	0.37	0.06	0.44	0.09	0.37	0.10
AuNS/pulp	0.53	0.41	0.06	0.32	0.07	0.53	0.08

[a] $O^* = O_\alpha + O_\beta + O_c$; $C^* = C_1 + C_2 + C_3 + C_4$.

Conclusions

In this work, an novel one-step approach to synthesize the smart paper transformer supported AuNS/pulp was developed for high-efficiency and high-reusability catalysis. After systematic studies of the composition, structure, and morphology of the AuNS/pulp catalyst by different characterization techniques such as XRD, TGA, FE-SEM, TEM, FT-IR, and XPS, the s-PAT supported AuNS/pulp was successfully used for efficient catalytic reduction of 4-NP with high reusability. The porous microstructures of the AuNS and paper and the uniform distribution of the AuNS catalyst in a solution by the s-PAT liquid phase all contributed to the high catalytic efficiency of the AuNS/pulp catalyst, while the transformation to the solid phase of s-PAT enabled exceptional reusability and regeneration capacity.

Notably, for the first time, we developed a novel noble metal nanocatalyst platform on a smart paper transformer based on the smart phase conversion of paper and demonstrated excellent catalytic efficiency and reusability of the platform in environmental catalytic applications. The smart transformation between the liquid phase of pulp and the solid phase paper of the s-PAT supported noble metal nanocatalysts ensures not only high catalytic efficiency but also excellent reusability. For instance, the conversion rate of 4-NP reached nearly 100% within 6 min under optimal conditions. The comparison between the AuNS/pulp and AuNS/paper catalysts indicated superior catalytic efficiency of the s-PAT supported AuNS/pulp compared to AuNS/paper. Furthermore, s-PAT can maintain high catalytic efficiencies even after many cycles of reuse. The AuNS/pulp catalyst still exhibited a high catalytic efficiency of 91.6% within 7 min in the fifteenth cycle of reuse for 4-NP reduction. Liquid-phase catalysts can exhibit high catalytic efficiency but not good reusability. In contrast, solid-phase catalysts can easily achieve high reusability but not high catalytic efficiency. Therefore, this innovative phase transformation solves a vital problem in the current field of catalysis by fusing high efficiency and outstanding reusability in the same nanocatalyst and sheds light on efficient and economical catalysis for many fields ranging from environmental remediation and organic synthesis to biomass conversion and large-scale industrial applications.[72]

Conflicts of interest

There are no conflicts to declare.

Acknowledgements

Notes and references

1 W. Zhang, G. Wang, Z. Y. He, C. Y. Hou, Q. H. Zhang, H. Z. Wang and Y. G. Li, *Mater. Des.*, 2016, **109**, 492–502.

2 M. Dou, S. T. Sanjay, D. C. Dominguez, S. Zhan and X. J. Li, *Chem. Commun.*, 2017, **53**, 10886–10889.

3 G. L. Fu, S. T. Sanjay, M. W. Dou and X. J. Li, *Nanoscale*, 2016, **8**, 5422–5427.

4 G. Q. Cheng, Y. Wang, K. Liu and J. H. Yu, *Nano Res.*, 2018, **11**, 1018–1028.

5 Z. Wu, D. E. Jiang, A. K. Mann, D. R. Mullins, Z. A. Qiao, L. F. Allard, C. Zeng, R. Jin and S. H. Overbury, *J. Am. Chem. Soc.*, 2014, **136**, 6111–6122.

6 H. L. Jiang, B. Liu, T. Akita, M. Haruta, H. Sakurai and Q. Xu, *J. Am. Chem. Soc.*, 2009, **131**, 11302–11303.

7 N. Agarwal, S. J. Freakley, R. U. McVicker, S. M. Althahban, N. Dimitratos, Q. He, D. J. Morgan, R. L. Jenkins, D. J. Willock, S. H. Taylor, C. J. Kiely and G. J. Hutchings, *Science*, 2017, **358**, 223–226.

8 S. K. Katla, J. Zhang, E. Castro, R. A. Bernal and X. J. Li, *ACS Appl. Mater. Interfaces*, 2018, **10**, 75–82.

9 B. K. Poudel, J. O. Kim and J. H. Byeon, *Adv. Sci.*, 2018, **5**, 1700563.

10 Q. Yang, J. R. Peng, Y. Xiao, W. T. Li, L. W. Tan, X. H. Xu and Z. Y. Qian, *ACS Appl. Mater. Interfaces*, 2018, **10**, 150–164.

11 T. J. Corrie, L. T. Ball, C. A. Russell and G. C. Lloyd-Jones, *J. Am. Chem. Soc.*, 2017, **139**, 245–254.

12 D. Han, Z. Bao, H. Xing, Y. Yang, Q. Ren and Z. Zhang, *Nanoscale*, 2017, **9**, 6026–6032.

13 J. W. Xia, Y. S. Fu, G. Y. He, X. Q. Sun and X. Wang, *Appl. Catal., B*, 2017, **200**, 39–46.

14 X. Y. Du, J. He, J. Zhu, L. J. Sun and S. S. An, *Appl. Surf. Sci.*, 2012, **258**, 2717–2723.

15 J. Lee, J. C. Park and H. Song, *Adv. Mater.*, 2008, **20**, 1523–1528.

16 H. Cavusoglu, B. Z. Buyukbekar, H. Sakalak and S. Kohsakowski, *Chemphyschem*, 2017, **18**, 1956.

17 Z. L. Yan, L. J. Fu, X. C. Zuo and H. M. Yang, *Appl. Catal., B*, 2018, **226**, 23–30.

18 W. Fang, Y. Deng, L. Tang, G. Zeng, Y. Zhou, X. Xie, J. Wang, Y. Wang and J. Wang, *J. Colloid Interface Sci.*, 2017, **490**, 834–843.

19 J. Fang, S. W. Cao, Z. Wang, M. M. Shahjamali, S. C. J. Loo, J. Barber and C. Xue, *Int. J. Hydrogen Energy*, 2012, **37**, 17853–17861.

20 N. Basavegowda, K. Mishra and Y. R. Lee, *J. Alloys Compd.*, 2017, **701**, 456–464.

21 P. An, R. Anumula, C. N. Cui, Y. Liu, F. Zhan, Y. Tao and Z. X. Luo, *Nano Res.*, 2019, **12**, 2589–2596.

22 J. Li, F. C. Wu, L. Lin, Y. Guo, H. O. Liu and X. F. Zhang, *Chem. Eng. J.*, 2018, **333**, 146–152.

23 X.-Q. Qiao, Z.-W. Zhang, F.-Y. Tian, D.-F. Hou, Z.-F. Tian, D.-S. Li and Q. Zhang, *Cryst. Growth Des.*, 2017, **17**, 3538–3547.

24 W. C. Ye, J. Yu, Y. X. Zhou, D. Q. Gao, D. A. Wang, C. M. Wang and D. S. Xue, *Appl. Catal., B*, 2016, **181**, 371–378.

25 J. Zhao, Y. Yu, X. L. Xu, S. X. Di, B. L. Wang, H. Xu, J. Ni, L. L. Guo, Z. Y. Pan and X. N. A. Li, *Appl. Catal., B*, 2017, **206**, 175–183.

26 F. Ke, L. Wang and J. Zhu, *Nanoscale*, 2015, **7**, 1201–1208.

27 X. Li, X. Wang, S. Song, D. Liu and H. Zhang, *Chem.–Eur. J.*, 2012, **18**, 7601–7607.

28 C. Gao, X. L. Wang, H. S. Wang, J. H. Zhou, S. R. Zhai and Q. D. An, *Int. J. Biol. Macromol.*, 2020, **144**, 947–953.

29 A. Elham, F. Mehrdad and R. G. Mohammad, *Mater. Chem. Phys.*, 2017, **198**, 374–379.

30 X. J. Yang, P. F. Tian, C. X. Zhang, Y. Q. Deng, J. Xu, J. L. Gong and Y. F. Han, *Appl. Catal., B*, 2013, **134**, 145–152.

31 Q. J. Jin, L. Ma, W. Zhou, C. Himmelhaver, R. Chintalapalle, Y. S. Shen and X. Li, *Catal. Today*, 2020, DOI: 10.1016/j.cattod.2020.01.023.

32 J. L. Wang, F. Y. Chen, Y. C. Jin and Y. M. Lei, *ACS Appl. Mater. Interfaces*, 2018, **10**, 6276–6287.

33 Y. Yan, A. I. Radu, W. Y. Rao, H. M. Wang, G. Chen, K. Weber, D. Wang, D. Cialla-May, J. Popp and P. Schaaf, *Chem. Mater.*, 2016, **28**, 7673–7682.

34 K. S. Prasad, X. Cao, N. Gao, Q. Jin, S. T. Sanjay, G. Henao-Pabon and X. Li, *Sens. Actuators, B*, 2020, **305**, 127516.

35 H. Mao, C. G. Ji, M. H. Liu, Z. Q. Cao, D. Y. Sun, Z. Q. Xing, X. Chen, Y. Zhang and X. M. Song, *Appl. Surf. Sci.*, 2018, **434**, 522–533.

36 Y. Gu, Y. Q. Jiao, X. G. Zhou, A. P. Wu, B. Buhe and H. G. Fu, *Nano Res.*, 2018, **11**, 126–141.

37 F. Wei, C. F. Lu, F. Y. Wang, G. C. Yang, Z. X. Chen and J. Q. Nie, *Mater. Lett.*, 2018, **212**, 251–255.

38 X. Y. An, Y. D. Long and Y. H. Ni, *Carbohydr. Polym.*, 2017, **156**, 253–258.

39 S. T. Sanjay, G. Fu, M. Dou, F. Xu, R. Liu, H. Qi and X. Li, *Analyst*, 2015, **140**, 7062–7081.

40 T. Kamal, S. B. Khan and A. M. Asiri, *Environ. Pollut.*, 2016, **218**, 625–633.

41 I. Ahmad, T. Kamal, S. B. Khan and A. M. Asiri, *Cellulose*, 2016, **23**, 3577–3588.

42 T. Kamal, S. B. Khan, S. Haider, Y. G. Alghamdi and A. M. Asiri, *Int. J. Biol. Macromol.*, 2017, **104**, 56–62.

43 T. Zeng, K. L. Ziegelgruber, Y. P. Chin and W. A. Arnold, *Environ. Sci. Technol.*, 2011, **45**, 6814–6822.

44 C. Lin, G. Wu, H. Li, Y. Geng, G. Xie, J. Yang, B. Liu and J. Jin, *Nanoscale*, 2017, **9**, 1834–1839.

45 V. K. Gupta, M. L. Yola, T. Eren, F. Kartal, M. O. Çağlayan and N. Atar, *J. Mol. Liq.*, 2014, **190**, 133–138.

46 B. Wang, X. L. Lv, D. Feng, L. H. Xie, J. Zhang, M. Li, Y. Xie, J. R. Li and H. C. Zhou, *J. Am. Chem. Soc.*, 2016, **138**, 6204–6216.

47 P. T. Huong, B.-K. Lee, J. Kim and C.-H. Lee, *Mater. Des.*, 2016, **101**, 210–217.

48 P. Garcia, M. Malacria, C. Aubert, V. Gandon and L. Fensterbank, *ChemCatChem*, 2010, **2**, 493–497.

49 J. J. Lv, S. S. Li, A. J. Wang, L. P. Mei, J. R. Chen and J. J. Feng, *Electrochim. Acta*, 2014, **136**, 521–528.

50 M. Kumar and S. Deka, *ACS Appl. Mater. Interfaces*, 2014, **6**, 16071–16081.

51 J. Li, C. Y. Liu and Y. Liu, *J. Mater. Chem.*, 2012, **22**, 8426.

52 Z. H. Ren, H. T. Li, Q. Gao, H. Wang, B. Han, K. S. Xia and C. G. Zhou, *Mater. Des.*, 2017, **121**, 167–175.

53 J. S. Wu, J. S. Wang, T. N. Wang, L. M. Sun, Y. C. Du, Y. L. Li and H. Y. Li, *Appl. Surf. Sci.*, 2019, **466**, 342–351.

54 J. Luo, N. Zhang, R. Liu and X. Y. Liu, *RSC Adv.*, 2014, **4**, 64816–64824.

55 L. P. Mei, R. Wang, P. Song, J. J. Feng, Z. G. Wang, J. R. Chen and A. J. Wang, *New J. Chem.*, 2016, **40**, 2315–2320.

56 M. W. Dou, S. T. Sanjay, M. Benhabib, F. Xu and X. J. Li, *Talanta*, 2015, **145**, 43–54.

57 S. T. Sanjay, M. W. Dou, J. J. Sun and X. J. Li, *Sci. Rep.*, 2016, **6**, 30474.

58 J. C. Cheng, S. L. Zhao, W. B. Gao, P. B. Jiang and R. Li, *React. Kinet., Mech. Catal.*, 2017, **121**, 797–810.

59 D. H. Wang, B. Zhao, Y. Jiang, P. F. Hu, D. D. Gao and H. J. Zhang, *Catal. Commun.*, 2017, **102**, 114–117.

60 T. Kondo and C. Sawatari, *Polymer*, 1996, **37**, 393–399.

61 M. Schwanninger, J. C. Rodrigues, H. Pereira and B. Hinterstoisser, *Vib. Spectrosc.*, 2004, **36**, 23–40.

62 D. Ruan, L. N. Zhang, Y. Mao, M. Zeng and X. B. Li, *J. Membr. Sci.*, 2004, **241**, 265–274.

63 X. Colom and F. Carrillo, *Eur. Polym. J.*, 2002, **38**, 2225–2230.

64 S. Y. Oh, D. I. Yoo, Y. Shin, H. C. Kim, H. Y. Kim, Y. S. Chung, W. H. Park and J. H. Youk, *Carbohydr. Res.*, 2005, **340**, 2376–2391.

65 Y. Cao and H. M. Tan, *J. Mol. Struct.*, 2004, **705**, 189–193.

66 M. Kacurakova, A. C. Smith, M. J. Gidley and R. H. Wilson, *Carbohydr. Res.*, 2002, **337**, 1145–1153.

67 S. B. Khan, F. Ali, T. Kamal, Y. Anwar, A. M. Asiri and J. Seo, *Int. J. Biol. Macromol.*, 2016, **88**, 113–119.

68 D. Kim, M. Jang, J. Seo, K.-H. Nam, H. Han and S. B. Khan, *Compos. Sci. Technol.*, 2013, **75**, 84–92.

69 S. B. Khan, K. A. Alamry, E. N. Bifari, A. M. Asiri, M. Yasir, L. Gzara and R. Z. Ahmad, *J. Ind. Eng. Chem.*, 2015, **24**, 266–275.

70 P. H. F. Pereira, H. J. C. Voorwald, M. O. H. Cioffi, M. Da Silva, A. M. B. Rego, A. M. Ferraria and M. N. De Pinho, *Cellulose*, 2014, **21**, 641–652.

71 P. Bazant, I. Kuritka, L. Munster and L. Kalina, *Cellulose*, 2015, **22**, 1275–1293.

72 S. Zhan, H. Zhang, Y. Zhang, Q. Shi, Y. Li and X. Li, *Appl. Catal., B*, 2017, **203**, 199–209.